

Weak lensing of the CMB

Duncan Hanson · Anthony Challinor · Antony
Lewis

Received: date / Accepted: date

Abstract The cosmic microwave background (CMB) represents a unique source for the study of gravitational lensing. It is extended across the entire sky, partially polarized, located at the extreme distance of $z = 1100$, and is thought to have the simple, underlying statistics of a Gaussian random field. Here we review the weak lensing of the CMB, highlighting the aspects which differentiate it from the weak lensing of other sources, such as galaxies. We discuss the statistics of the lensing deflection field which remaps the CMB, and the corresponding effect on the power spectra. We then focus on methods for reconstructing the lensing deflections, describing efficient quadratic maximum-likelihood estimators and delensing. We end by reviewing recent detections and observational prospects.

Keywords Cosmic Microwave Background; Gravitational Lensing

1 Introduction

1.1 *What is the CMB?*

The cosmic microwave background (CMB) is a blackbody radiation which permeates the Universe. It was released approximately 400,000 years after the Big Bang, when the primordial plasma had cooled enough that neutral hydrogen atoms could form, and the Universe became effectively transparent to radiation. To a very good degree of approximation, the CMB temperature is uniform across the sky, with a value today of 2.725 K [1]. At the level of one part in 10^5 , however, the CMB temperature has small anisotropies which are due to fluctuations of density and bulk velocity in the

D. Hanson · A. Challinor · A. Lewis

Institute of Astronomy and Kavli Institute for Cosmology Cambridge, Madingley Road, Cambridge, CB3 0HA, UK

E-mail: dhanson@ast.cam.ac.uk

A. Challinor

DAMTP, Centre for Mathematical Sciences, Wilberforce Road, Cambridge CB3 0WA, UK

primordial plasma. The measurement of these anisotropies is clearly a difficult task, but a number of very successful experiments have driven rapid progress in this field over the past two decades. Modern temperature experiments such as ACT¹, SPT², and Planck³ are now pushing to robust arcminute-scale measurements, while polarization experiments like Spider⁴, QUIET⁵, BICEP2 and Planck⁶ will soon obtain low-noise maps of the CMB polarization. Gravitational lensing effects should become readily apparent in both types of observation, requiring detailed modelling to interpret the data correctly, but also offering additional information about the Universe at intermediate redshifts.

1.2 What is special about the CMB in the context of lensing?

In the context of lensing, the CMB can be thought of as a single source “plane” with several unique features:

1. It is extended across the entire sky.
2. It probes the matter distribution at relatively higher redshifts ($z \sim 2$) than can be studied with e.g. galaxy lensing: the last-scattering surface from which the CMB was released ($z \sim 1100$) is the most distant light source we will ever be able to see.
3. It is partially linearly polarized, which provides two additional lensed observables. The local quadrupole of the radiation field at the last scattering surface generates linear polarization through the mechanism of Thomson scattering, at a level of 10% of the temperature anisotropies [2]. The observable CMB is therefore characterized by three numbers as a function of position on the sky – the total radiation intensity, and two Stokes parameters describing the amplitude and direction of the linear polarization.
4. To a good degree of approximation the source fluctuations may be treated as those of a Gaussian random field. The signal along any particular direction is essentially random, but the correlations between directions at different angular separations is encoded in the power spectrum, which completely characterizes the signal. A typical CMB temperature realization, for example, is plotted in Fig. 1.

1.3 Why study CMB lensing?

To someone interested in the primary CMB, the lensing of the CMB is important as a contaminant. As we will discuss in Sec. 4, lensing has a small but non-negligible effect on the CMB power spectra, and must be accounted for in modern parameter

¹ <http://www.physics.princeton.edu/act/>

² <http://pole.uchicago.edu/>

³ <http://www.rssd.esa.int/index.php?project=planck>

⁴ http://www.astro.caltech.edu/~lgg/spider_front.htm

⁵ <http://quiet.uchicago.edu/>

⁶ <http://www.rssd.esa.int/index.php?project=planck>

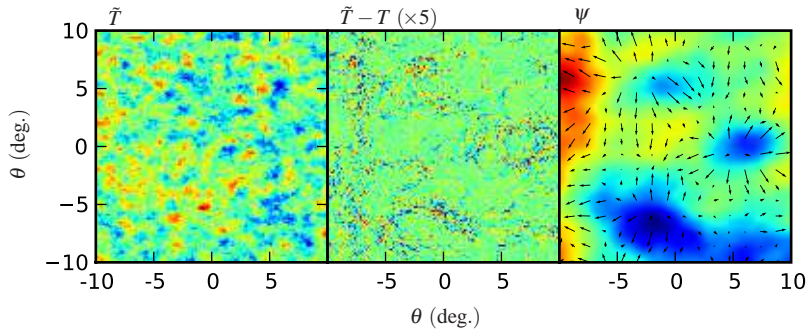


Fig. 1 Left: lensed CMB realization. Middle: difference map between lensed and unlensed CMB. Right: realization of ψ for the lensing, and an overlay of its gradient, the deflection angle.

analyses to obtain unbiased constraints. Perhaps more importantly, lensing effects generate a curl-like (B mode) polarization pattern on the sky which acts as a limiting source of confusion for low-noise polarization experiments targeting the signal from primordial gravitational waves [3,4]. This confusion can be reduced with an accurate cleaning of the lensing-induced signal, which we will discuss in Sec. 5.

Apart from being a nuisance for traditional observables, the lensing of the CMB can act as an additional source of information. A typical analysis of the CMB assumes Gaussianity and statistical isotropy, in which case the power spectrum is the only quantity of interest. As we shall discuss, lensing can be thought of as introducing into the CMB small amounts of non-Gaussianity (when marginalized over realizations of the lenses) or statistical anisotropy (for a fixed distribution of lenses). This effectively *introduces* information into the CMB, contained in the higher-order statistics (for the non-Gaussian viewpoint) and the off-diagonal elements of its covariance matrix (for the anisotropy viewpoint). With only one CMB sky to observe and interpret, both these viewpoints are useful. The additional information from lensing probes the state of the Universe at intermediate redshifts ($z \sim 2$). This can be used to break parameter degeneracies and place improved constraints on quantities that affect the geometry or density perturbations at late times, such as the dark energy equation of state and portion of the energy budget in massive neutrinos. An optimal analysis of lensing effects with the data from the Planck satellite, for example, will enable us to measure the sum of neutrino masses to ~ 0.1 eV, while lens reconstruction with a next-generation polarization mission such as EPIC/CMBPol can constrain the sum to 0.05 eV or better [5,6,7]. This is an interesting limit, close to the minimum value for the sum of the masses suggested by terrestrial oscillation measurements in the normal hierarchy.

2 Observables

Here we will briefly review the mathematical description of CMB observables and establish our notation. Throughout this review we will use an overtilde to represent lensed quantities. For quantitative calculations we assume that the Universe is described by a flat, concordance Λ CDM cosmology with parameters given by the WMAP 5-year best-fit model.

The CMB radiation pattern on the sky is conveniently expressed in terms of the Stokes parameters T , Q and U , which are measures of the total intensity (T ; here expressed as an equivalent blackbody temperature relative to the background, uniform CMB) and linear polarization (Q and U). Rotation of the measurement coordinates does not affect T , however the Q and U Stokes parameters mix according to

$$[Q \pm iU]_{\xi} = e^{\pm 2i\xi} [Q \pm iU]_0, \quad (1)$$

where ξ is the angle of the rotation⁷. Thus, $Q \pm iU$ is a spin ± 2 quantity. A rotation of 45 degrees converts $Q \rightarrow U$, and a 90-degree rotation results in a sign flip. For more information on this notation, see for example [8].

The statistics of the CMB are often simplest to study as a function of scale rather than angular position. On a patch of the sky which is small enough that it may be treated as flat, the Fourier modes provide an appropriate basis. In this review, we will take the convention that

$$\begin{aligned} T(\mathbf{l}) &= \int \frac{d^2\mathbf{x}}{2\pi} T(\mathbf{x}) e^{-i\mathbf{l}\cdot\mathbf{x}} \\ [E(\mathbf{l}) \pm iB(\mathbf{l})] &= - \int \frac{d^2\mathbf{x}}{2\pi} [Q \pm iU] e^{\mp 2i\xi_1} e^{-i\mathbf{l}\cdot\mathbf{x}}. \end{aligned} \quad (2)$$

Here ξ_1 is the angle between \mathbf{l} and the x -axis. The placement of the $e^{\mp 2i\xi_1}$ factor in the polarization transform rotates the Fourier transforms of the Stokes parameters to a basis adapted to the Fourier wavevector, resulting in E and B fields which are spin-0. This makes E and B independent of any measurement conventions, and so they are the natural basis to perform calculations in. The E/B -mode decomposition is also useful for studying the origin of fluctuations in the early Universe: B -modes are not generated by scalar perturbations, and so the detection of non-zero primordial B -mode power could in principle be a ‘‘smoking gun’’ for primordial tensor modes [9, 10].

The primary, unlensed CMB fluctuations are thought to be well approximated as a statistically-isotropic Gaussian random field with zero mean. This means that in the Fourier domain, each mode is drawn from a (complex) Gaussian, with variance which depends only on the length of the wavevector, and not on its direction. The length-dependent part is known as the power spectrum C_l . In the Fourier basis, for example we have

$$\langle X(\mathbf{l}) Z^*(\mathbf{l}') \rangle = \delta(\mathbf{l} - \mathbf{l}') C_l^{XZ}, \quad (3)$$

⁷ This is for Stokes parameters defined on a right-handed x - y basis with z along the propagation direction, and for a left-handed rotation about z .

where X, Z can be T, E or B , and $l = |\mathbf{l}|$. If parity is respected in the mean, C_l^{TB} and C_l^{EB} must vanish, but note that there is a non-zero cross-correlation between the temperature and the E -mode polarization. Because the modes are drawn from a Gaussian distribution, they are completely characterized by their two-point statistics. Higher order odd-point functions are zero, and the even-point functions can be computed from the power spectra using Wick's theorem.

We now proceed to describe the large-scale structures responsible for the lensing of the CMB.

3 Lensing potential

3.1 Lensing deflection

The effect of lensing on the CMB can be described in the flat-sky limit as a remapping of the primary (unlensed) CMB given by

$$\tilde{T}(\mathbf{x}) = T(\mathbf{x} + \alpha(\mathbf{x})) \quad (4)$$

$$[\tilde{Q} \pm i\tilde{U}](\mathbf{x}) = [Q \pm iU](\mathbf{x} + \alpha(\mathbf{x})) \quad (5)$$

where $\alpha(\mathbf{x})$ is a field of deflection vectors.

The observed deflection vector is given by a sum of all the deflections by lenses between ourselves and the last scattering surface; mathematically this is given by an integral over the standard weak lensing equation along the photon path. In a flat universe, and under the Born approximation (taking the integral along the unperturbed path) we have

$$\alpha(\mathbf{x}) = -2 \int_0^{\chi_*} d\chi \frac{\chi_* - \chi}{\chi_*} \nabla_{\perp} \Psi(\chi \mathbf{x}; \eta_0 - \chi), \quad (6)$$

where Ψ is the Weyl potential, χ_* is the conformal distance to last scattering, and η_0 is the conformal time today. Here, the gradient is taken transverse to the propagation direction. In Einstein gravity with vanishing anisotropic stresses, the Weyl potential is simply the Newtonian potential. More generally, in any metric theory of gravity, Ψ is given in terms of the Newtonian-gauge potentials ϕ_N and ψ_N by $\Psi = (\phi_N + \psi_N)/2$: it is the scalar field which determines the Weyl tensor (non-local part of the Riemann tensor) in the presence of scalar perturbations. For further details and the simple generalization to a non-flat Universe see [11].

3.2 Order of magnitude

It is useful to get a feel for the order of magnitude of the lensing effect on the CMB, and why it is important. We can think of the large scale structure of the Universe as a collection of potential wells, crudely approximated as those due to point-source masses. Each gives an observed deflection angle of

$$|\alpha^{\text{ps}}(\mathbf{x})| = 4 \left(\frac{\chi_* - \chi}{\chi_*} \right) \Psi^{\text{ps}}(\chi \mathbf{x}), \quad (7)$$

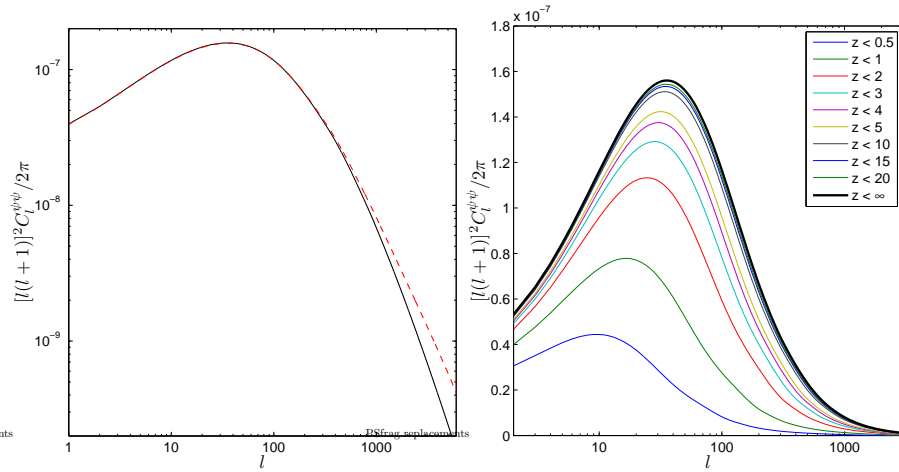


Fig. 2 Left: angular power spectrum of the lensing deflection angle in linear theory (solid), and with the HALOFIT non-linear corrections given by Eq. (14) (dashed). Right: cumulative contributions to the power spectrum as a function of maximum redshift.

where χ is the conformal distance to the point source and $\Psi^{\text{ps}}(\chi\mathbf{x})$ is the potential at closest approach. Thus nearby lenses have the largest contribution from the geometric factor $(\chi_* - \chi)/\chi_*$, though the linear potentials are actually somewhat smaller at low redshift due to the suppression of perturbation growth by the dark energy. During matter domination the geometric factor is given by $(1 - \chi/\chi_*) \sim [1/(1+z)]^{1/2}$, which depends somewhat weakly on redshift, so we will ignore it for the rest of this order-of-magnitude calculation.

The potentials are nearly scale-invariant on large scales, but become small on scales below the turnover in the matter power spectrum. We therefore need to consider lensing by perturbations from the largest observable scale $\sim \chi_* \sim 14000 \text{ Mpc}$ down to $\sim 300 \text{ Mpc}$. The number of lenses along the line of sight also depends on scale: there is only one of the largest lenses, but $\sim 14000/300 \sim 50$ of the smallest ones, so the smaller lenses contribute most to the lensing deflection. The size of each deflection is set by the Newtonian potentials, which have variance $\sim (2.7 \times 10^{-5})^2$ per unit log range in scale, so typical deflections have $|\alpha| \sim 10^{-4}$. Taking each lens to be independent, the total r.m.s. deflection should therefore be $\sim 50^{1/2} \times 10^{-4} \sim 7 \times 10^{-4}$, or about 2 arcmin.

The coherence scale of the deflection field is given by the angular extent of a typical 300 Mpc structure. At a distance $\chi = 7000 \text{ Mpc}$ (halfway to the last-scattering surface) this is $(300/7000) \sim 2^\circ$.

These order of magnitude estimates are borne out by more accurate calculations. The RMS deflection angle for the WMAP 5-year cosmology is 2.7 arcmin. The scale dependence (i.e. angular power spectrum) and cumulative redshift dependence of the deflection power are shown in Fig. 2. Nearby objects tend to contribute to the lensing potential on larger angular scales. The deflection power peaks in the region $20 < l < 100$, corresponding to a coherence length of a few degrees.

3.3 Lensing potential

Rather than using the deflection field directly, weak lensing studies are often cast in terms of the magnification matrix A_{ij} defined by

$$A_{ij} \equiv \delta_{ij} + \frac{\partial}{\partial \theta_i} \alpha_j = \begin{pmatrix} 1 - \kappa - \gamma_1 & -\gamma_2 + \omega \\ -\gamma_2 - \omega & 1 - \kappa + \gamma_1 \end{pmatrix}, \quad (8)$$

where the quantities κ , $\gamma_1 + i\gamma_2$, and ω are known as the convergence, (complex) shear, and field rotation respectively. In galaxy lensing the magnification matrix is useful because in many cases this can be approximated as being constant over the angular extent of the source. Shear then produces an additional elliptical distortion of the projected shapes of galaxies, while convergence changes their apparent size and density on the sky. For galaxy lensing the shear is the more useful observable since observing the convergence would require knowledge of the unlensed distribution of galaxies. In CMB lensing, the degree-scale acoustic features are large compared to the coherence size of the magnification matrix, so the latter cannot be assumed constant over typical CMB features. Moreover, the statistics of the source plane are well known (the CMB is nearly a Gaussian random field), and so the convergence is just as useful as shear. For these reasons CMB lensing studies usually work directly with the lensing deflection field as a function of position on the sky, rather than using the magnification matrix.

From Eq. (6) we know that the deflection field is a sum of projected gradient terms. Approximating the light path by the unperturbed line of sight, the deflection field can be expressed as an angular gradient. In detail, relating the projected and angular gradients at distance χ via $\nabla_{\perp} \Psi = (\nabla \Psi) / \chi$, we can define a lensing potential $\psi(\mathbf{x})$ so that

$$\alpha(\mathbf{x}) = \nabla \psi(\mathbf{x}), \quad (9)$$

where the derivative is now with respect to position on the sky. The lensing potential can be calculated as the line-of-sight integral

$$\psi(\mathbf{x}) = -2 \int_0^{\chi_*} d\chi \left(\frac{\chi_* - \chi}{\chi_* \chi} \right) \Psi(\chi \mathbf{x}; \eta_0 - \chi). \quad (10)$$

To what extent is the deflection angle approximated by Eq. (10) valid? The major assumption was the Born approximation, which takes the integral of Eq. (10) along the unperturbed path. This will be a good approximation if the deflection angles are sufficiently small, or if all of the lensing occurs in a single thin plane. The dependence of the lensing potential on this assumption can be investigated quantitatively under the second-order Born approximation – taking the gravitational potential along the perturbed path given by the first-order result. The effect on the gradient component of $\alpha(\mathbf{x})$ is computed in [12, 13], and is expected to be negligible for any future experiment. A potentially more important aspect of the second-order Born approximation is that it introduces a non-zero curl component into the deflection field, however this is not expected to be significant for experimental noise levels achievable in planned future surveys (i.e. greater than $0.25 \mu\text{K-arcmin}$) [14]. The validity of the Born approximation can also potentially be investigated by ray-tracing through numerical simulations [15], although this has not yet been done.

3.4 Lensing potential power spectrum

The lensing potential depends on the geometry of the universe and the gravitational potential along the line of sight, and hence, like galaxy lensing, is a probe of cosmology. Assuming linear evolution from the primordial density fluctuations, we can take Ψ in Fourier space to be given by

$$\Psi(\mathbf{k}, \eta) = T_\Psi(k; \eta) \mathcal{R}(\mathbf{k}), \quad (11)$$

where $T_\Psi(k; \eta)$ is the transfer function, and $\mathcal{R}(\mathbf{k})$ are the primordial curvature fluctuations, with 3D power spectrum $\mathcal{P}_{\mathcal{R}}(\mathbf{k})$. Under this assumption, expanding $\psi(\mathbf{x})$ in harmonic space and taking the angular power spectrum gives [11]

$$C_l^{\Psi\Psi} = 16\pi \int \frac{dk}{k} \mathcal{P}_{\mathcal{R}}(k) \left[\int_0^{\chi_*} d\chi T_\Psi(k; \eta_0 - \chi) j_l(k\chi) \left(\frac{\chi_* - \chi}{\chi_* \chi} \right) \right]^2, \quad (12)$$

where $j_l(k\chi)$ is a spherical Bessel function. The *deflection* power spectrum, $l(l+1)C_l^\Psi$, for a typical model is plotted in Fig. 2. It is customary to plot $[l(l+1)]^2 C_l^{\Psi\Psi} / (2\pi)$ because

$$\int d\ln l \frac{[l(l+1)]^2 C_l^{\Psi\Psi}}{2\pi} \approx \langle \alpha \rangle^2, \quad (13)$$

the variance of the deflections.

The assumption of linear theory and Gaussian primordial fluctuations implies that Ψ is Gaussian as well. However, on small scales it is clear that the potentials are subject to a large degree of non-linear evolution. Fortunately, the size threshold for non-linearity is small enough that there are many such non-linear clumps on the way to the last-scattering surface. This Gaussianizes the projection of Ψ to some extent, but the non-linearity does still appear as an enhanced power spectrum, $C_l^{\Psi\Psi}$, on small scales; see Fig. 2. Non-linearity may therefore be approximately accounted for by scaling the linear transfer functions according to

$$T_\Psi(k, \eta) \rightarrow T_\Psi(k, \eta) \sqrt{\frac{\mathcal{P}_\Psi^{\text{non-linear}}(k; \eta)}{\mathcal{P}_\Psi(k; \eta)}}. \quad (14)$$

The non-linear power spectrum can be calculated from analytical fitting formulae such as those of HALOFIT [16]; this approach is implemented in the CAMB code [17]. The ultimate test of the Gaussian approximation is to propagate CMB photons through large numerical N -body simulations. Several groups have developed methods for creating the concentric-shell mass maps necessary to perform the radial integral of Eq. (6) numerically [15, 18, 19], and all find that the HALOFIT approach works well at the percent level for $l < 2000$.

4 Lensing effects on CMB observables

In Fig. 1 we show the difference between the lensed and unlensed sky for a realization of the CMB temperature. In this picture, the effect of lensing is to create a

non-Gaussian “boiling soup” pattern in the observed CMB. Large-scale lenses create coherent displacements across large patches of the sky, which appear as a modulation of the gradient of the unlensed CMB in the difference map.

To study the properties of the lensed CMB analytically, it is often useful to use a Taylor expansion of the lensing displacements. With the CMB temperature, for example, we have

$$\begin{aligned}\tilde{T}(\mathbf{x}) &= T(\mathbf{x} + \boldsymbol{\alpha}(\mathbf{x})) \\ &= T(\mathbf{x}) + \alpha^a \nabla_a T(\mathbf{x}) + \frac{1}{2} \alpha^a \alpha^b \nabla_a \nabla_b T(\mathbf{x}) + \dots\end{aligned}\quad (15)$$

The first line is not strictly correct outside the flat-sky approximation due to the curvature of the sky, however the Taylor expansion of the second line is, provided that the gradients are treated as covariant derivatives. This is also true for polarization provided that the polarization tensor is used in place of T [20].

The expansion in Eq. (15) is frequently useful to gain intuition into lensing effects. Consider, for example, the first-order expansion written in harmonic space:

$$[\alpha^a \nabla_a T](\mathbf{l}) = [\nabla^a \psi \nabla_a T](\mathbf{l}) = - \int \frac{d^2 \mathbf{L}}{2\pi} \mathbf{L}' \cdot (\mathbf{l} - \mathbf{L}) \psi(\mathbf{L}) T(\mathbf{l} - \mathbf{L}). \quad (16)$$

Here we can see that a mode of $\psi(\mathbf{L})$ with wavevector \mathbf{L} couples the unlensed CMB at wavevector $\mathbf{l} - \mathbf{L}$ into the observed CMB at wavevector \mathbf{l} . For fixed lenses, this mode-coupling introduces off-diagonal components into the covariance matrix of the observed CMB, with a characteristic spacing of $\delta l = 50$ given by the peak of the deflection angle power spectrum. Specifically,

$$\langle \tilde{T}(\mathbf{l}_1) \tilde{T}(\mathbf{l}_2) \rangle_{\text{CMB}} = \frac{1}{2\pi} \psi(\mathbf{l}_1 + \mathbf{l}_2) \cdot [\mathbf{l}_1 C_{l_1}^{TT} + \mathbf{l}_2 C_{l_2}^{TT}] \quad (\mathbf{l}_1 \neq \mathbf{l}_2), \quad (17)$$

where the average is over an ensemble of CMB fluctuations for fixed lenses. This is an interesting feature; large-wavelength modes of the lensing potential introduce correlations between CMB modes on much smaller scales. In Sec. 5 we will see how a reconstruction of the lensing potential can be made by correlating a large number of small-scale modes.

We note that the convergence of the lensing Taylor expansion is somewhat suspect – the typical RMS deflection angle of ~ 3 arcmin is comparable to the 10 arcmin scale length of modes at $l = 1000$, and so the expansion converges slowly at the map level. Nevertheless, when calculating ensemble-averaged quantities the lensing Taylor expansion is often quite accurate. In this case, it is relative displacements rather than the actual lensing effects which are important, and the Taylor expansion captures these reasonably well [21]. However the expansion is not accurate enough for a percent-level calculation of the lensed power spectrum.

4.1 Power spectra

The CMB power spectra completely characterize the primary fluctuations for Gaussian, statistically-isotropic models. Even though the lensed sky is slightly non-Gaussian,

the lensed power spectra are still useful for comparison with observations. Here we discuss the calculation of the lensed power spectra using the Taylor-series expansion described above. A more accurate non-perturbative result may be derived using correlation functions [22, 23, 24], however the Taylor approach gives more intuitive results and is less mathematically involved.

We will begin with temperature. For the purposes of compact notation, it is useful to write the lensing Taylor expansion schematically as

$$\tilde{T}(\mathbf{l}) = T(\mathbf{l}) + \delta T(\mathbf{l}) + \delta^2 T(\mathbf{l}) + \dots, \quad (18)$$

where the power of delta indicates the order in the lensing potential. The power spectrum to lowest order in $C_l^{\psi\psi}$ then follows from

$$C_l^{\tilde{T}\tilde{T}} \delta(\mathbf{l}-\mathbf{l}') \approx C_l^{TT} \delta(\mathbf{l}-\mathbf{l}') + \langle \delta T(\mathbf{l}) \delta T^*(\mathbf{l}') \rangle + \langle T(\mathbf{l}) \delta^2 T^*(\mathbf{l}') \rangle + \langle \delta^2 T(\mathbf{l}) T^*(\mathbf{l}') \rangle. \quad (19)$$

In the flat-sky approximation, the gradient operations are easily taken in Fourier space: $\delta T(\mathbf{l})$ is given by Eq. (16) while [25]

$$\delta^2 T(\mathbf{l}) = -\frac{1}{2} \int \frac{d^2 \mathbf{l}_1}{2\pi} \int \frac{d^2 \mathbf{l}_2}{2\pi} \mathbf{l}_1 \cdot (\mathbf{l}_1 + \mathbf{l}_2 - \mathbf{l}) \mathbf{l}_1 \cdot \mathbf{l}_2 T(\mathbf{l}_1) \psi(\mathbf{l}_2) \psi^*(\mathbf{l}_1 + \mathbf{l}_2 - \mathbf{l}), \quad (20)$$

from which the power spectrum may be derived. Assuming that both $T(\mathbf{l})$ and $\psi(\mathbf{l})$ have the statistics of an isotropic, Gaussian random field we find:

$$\langle T(\mathbf{l}) \delta^2 T^*(\mathbf{l}') \rangle + \langle \delta^2 T(\mathbf{l}) T^*(\mathbf{l}') \rangle = -l^2 R^\psi C_l^{TT} \delta(\mathbf{l}-\mathbf{l}') \quad (21)$$

$$\langle \delta T(\mathbf{l}) \delta T^*(\mathbf{l}') \rangle = \delta(\mathbf{l}-\mathbf{l}') \int \frac{d^2 \mathbf{L}}{(2\pi)^2} [\mathbf{L} \cdot (\mathbf{l}-\mathbf{L})]^2 C_{|\mathbf{l}-\mathbf{L}|}^{\psi\psi} C_L^{TT} \quad (22)$$

where R^ψ is half of the total mean-squared deflection,

$$R^\psi \equiv \frac{1}{2} \langle |\nabla \psi|^2 \rangle = \frac{1}{4\pi} \int \frac{dl}{l} l^4 C_l^{\psi\psi} \sim 3 \times 10^{-7}. \quad (23)$$

Assembling these results together, we find the lensed temperature power spectrum to first-order in $C_l^{\psi\psi}$

$$C_l^{\tilde{T}\tilde{T}} = (1 - l^2 R^\psi) C_l^{TT} + \int \frac{d^2 \mathbf{l}'}{(2\pi)^2} [\mathbf{l}' \cdot (\mathbf{l}-\mathbf{l}')]^2 C_{|\mathbf{l}-\mathbf{l}'|}^{\psi\psi} C_{l'}^{TT}. \quad (24)$$

The second term, which represents a convolution of the unlensed temperature power spectrum with the lensing potential power spectrum, almost cancels the R^ψ term over the acoustic part of the spectrum, leaving only a small blurring of the acoustic peaks with a characteristic kernel width of $\delta l \sim 50$. This is illustrated in Fig. 3, where we plot the lensed and unlensed spectra.

The unlensed CMB has very little power on small scales, $l > 3000$, due to diffusion damping. Deep enough into the damping tail, any non-negligible contribution to Eq. (24) from the unlensed temperature power spectrum will be from modes with $l' \ll l$, and so the lensed spectrum may be simplified as [25, 26]

$$C_l^{\tilde{T}\tilde{T}} \approx C_l^{\psi\psi} \int \frac{d^2 \mathbf{l}'}{(2\pi)^2} (\mathbf{l}' \cdot \mathbf{l})^2 C_{l'}^{TT} \approx l^2 C_l^{\psi\psi} \int \frac{dl'}{l'} \frac{(l')^4 C_{l'}^{TT}}{4\pi} \approx l^2 C_l^{\psi\psi} R^T, \quad (25)$$

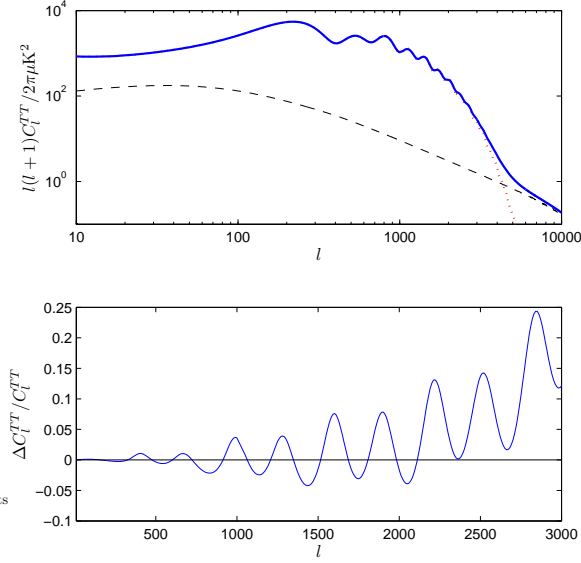


Fig. 3 Top: the lensed (solid) and unlensed (dotted) temperature power spectrum, as well as the small-scale approximation of Eq. (25) (dashed). Bottom: the fractional change in the power spectrum due to lensing.

where R^T is defined analogously to R^Ψ in Eq. (23), and is half the mean-squared gradient of the unlensed CMB. This causes an increase in the lensed CMB power of $\sim 10\%$ at $l > 2000$, as we can see in Fig. 3. Qualitatively, there are therefore two lensing effects on the temperature power spectrum: large-scale lenses smooth the peaks of the observed power spectrum, while small-scale lenses introduce small-scale power in the damping tail by lensing of the large-scale temperature gradient.

We now turn to the lensed polarization power spectra. For simplicity, we will assume that $B(\mathbf{l}) = 0$, i.e. that there are no primordial B -modes. In the flat-sky limit, lensing remaps the Stokes parameters defined on a fixed basis in the same way as for the temperature. The calculation is therefore similar to the temperature case, with the lensed spectra to lowest order in $C_l^{\Psi\Psi}$ given by [25]

$$C_l^{\tilde{T}\tilde{E}} = (1 - l^2 R^\Psi) C_l^{TE} + \int \frac{d^2\mathbf{l}'}{(2\pi)^2} [\mathbf{l}' \cdot (\mathbf{l} - \mathbf{l}')]^2 C_{|\mathbf{l} - \mathbf{l}'|}^{\Psi\Psi} C_{l'}^{TE} \cos[2(\xi_{l'} - \xi_{\mathbf{l}})] \quad (26)$$

$$C_l^{\tilde{E}\tilde{E}} = (1 - l^2 R^\Psi) C_l^{EE} + \int \frac{d^2\mathbf{l}'}{(2\pi)^2} [\mathbf{l}' \cdot (\mathbf{l} - \mathbf{l}')]^2 C_{|\mathbf{l} - \mathbf{l}'|}^{\Psi\Psi} C_{l'}^{EE} \cos^2[2(\xi_{l'} - \xi_{\mathbf{l}})] \quad (27)$$

$$C_l^{\tilde{B}\tilde{B}} = \int \frac{d^2\mathbf{l}'}{(2\pi)^2} [\mathbf{l}' \cdot (\mathbf{l} - \mathbf{l}')]^2 C_{|\mathbf{l} - \mathbf{l}'|}^{\Psi\Psi} C_{l'}^{EE} \sin^2[2(\xi_{l'} - \xi_{\mathbf{l}})], \quad (28)$$

where R^Ψ was defined in Eq. (23). Lensing of purely E -modes therefore generates B -mode polarization, even when there is none initially.

The lensing of the E -mode power spectrum, and the TE spectrum, is qualitatively similar to that of temperature. There is a convolution which blurs the features of the spectrum and shifts power into the damping tail. Quantitatively, the magnitude of the

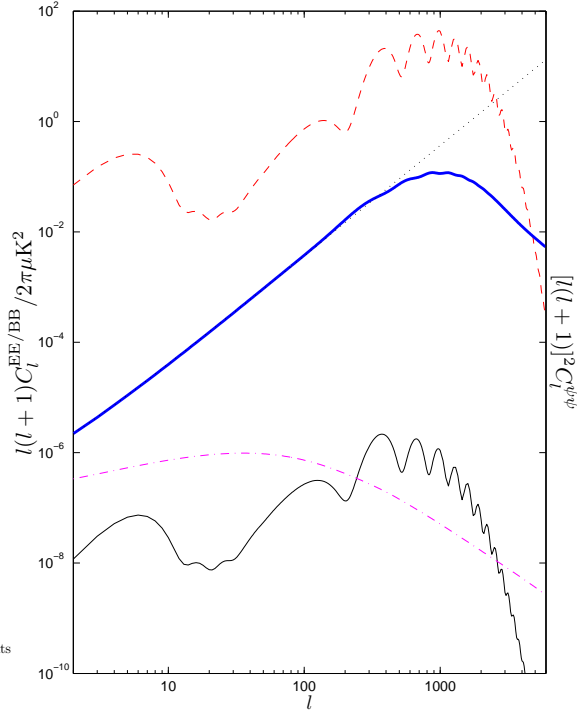


Fig. 4 The unlensed E -mode power spectrum $l(l+1)C_l^{EE}/2\pi$ (top; dashed), lensing deflection power spectrum $[l(l+1)]^2 C_l^{\psi\psi}$ (dot-dashed), and the contribution to the large-scale lensed B -mode power spectrum from each $\log l$ given by half their product (thin solid). The dotted line is the large-scale white spectrum $l(l+1)C_l^{\bar{B}\bar{B}}/2\pi$ given by Eq. (29), which can be compared to the full numerical result (thick solid). The lensed B -mode power spectrum has a close-to-white spectrum at $l \ll 1000$.

lensing effects is larger for the E -modes than for temperature, because the peaks in the unlensed power spectrum are rather sharper, leading to larger fractional changes in the lensed power of $\mathcal{O}(30\%)$ near the acoustic peaks [23, 24, 25].

Lensing of the CMB polarization causes power to leak from E - to B -modes, and this may be an important contaminant in the search for primordial B -modes on large angular scales. Since the unlensed E -mode spectrum peaks around $l \sim 1000$ (see Fig. 4), for $l \ll 1000$ we can take $|\mathbf{l}'| \gg |\mathbf{l}|$ in Eq. (28) giving

$$\begin{aligned} C_l^{\bar{B}\bar{B}} &\approx \int \frac{d^2\mathbf{l}'}{(2\pi)^2} |\mathbf{l}'|^4 C_{l'}^{\psi\psi} C_{l'}^{EE} \sin^2 2(\xi_{l'} - \xi_l) \\ &= \frac{1}{4\pi} \int \frac{dl'}{l'} l'^4 C_{l'}^{\psi\psi} l'^2 C_{l'}^{EE}. \end{aligned} \quad (29)$$

This is independent of l , corresponding to a white-noise spectrum of B -modes. In Fig. 4 we can see that the lensed B -modes are nearly white for $l < 100$, with the level predicted by Eq. (29). For the fiducial model we have $C_l^{\bar{B}\bar{B}} \sim 2 \times 10^{-6} \mu\text{K}^2$, corresponding to an instrumental white-noise level of $\sim 5 \mu\text{K}\text{-arcmin}$. The next gen-

eration of polarization surveys should achieve noise levels close to this and lensing will therefore become an important source of confusion for them.

To assess the amount of additional cosmological information in the lensed spectra over the unlensed, consider attempting to constrain departures of $C_l^{\psi\psi}$ from some fiducial spectrum:

$$C_l^{\psi\psi} = (1 + f_l)C_l^{\psi\psi}|_{\text{fid.}}. \quad (30)$$

An eigenmode analysis of the Fisher matrix for this problem can be used to identify modes of f_l which are constrained well by data. For a cosmic-variance limited experiment to $l_{\text{max}} = 2000$, there are essentially two such modes [27]. From the TT and EE power spectra, there is a mode which peaks at $l = 100$ and tracks the dominant lensing power. These are the modes of $C_l^{\psi\psi}$ which smooth the observed power spectra. Including B -mode polarization, there is a second mode which is much broader, reflecting the fact that the large scale B -mode power is sourced by lenses on all scales. This mode peaks at $l = 200$, but has a broad tail extending past $l = 1000$.

Increasing the l_{max} of the temperature measurement beyond $l = 2000$, the small-scale modes of the lensing potential would ideally also be constrained by the increase in the small-scale lensed power which they cause. However, in this regime extra-Galactic foregrounds and secondary effects will provide a source of confusion which is, as yet, not well understood.

The amplitude of the well-constrained $C_l^{\psi\psi}$ modes is somewhat dependent on cosmology, and so they may be used to place improved constraints on parameters. Some care is required with the B -mode power spectrum due to the highly non-Gaussian nature of the lens-induced B -modes leading to correlations between estimates of $C_l^{\tilde{B}\tilde{B}}$ at different scales [27, 28, 29]. On the whole, the power spectra are a rather sub-optimal statistic for extracting information from CMB lensing, however. Improved constraints can be made with estimators which are designed specifically to detect the lensing signal; these are discussed in Sec. 5.

4.2 Bispectra

The bispectrum, or three-point correlation function is given by

$$\langle \tilde{T}(\mathbf{l}_1)\tilde{T}(\mathbf{l}_2)\tilde{T}(\mathbf{l}_3) \rangle = \tilde{B}(\mathbf{l}_1, \mathbf{l}_2, \mathbf{l}_3)\delta(\mathbf{l}_1 + \mathbf{l}_2 + \mathbf{l}_3). \quad (31)$$

It is the simplest, lowest-order statistic which can be used to test for a skewed non-Gaussianity of the CMB fluctuations and so it has received much attention (see [30] for a review). Considering the effects to second order in the lensing potential, the lensed bispectrum is given in terms of the unlensed bispectrum by

$$\begin{aligned} \tilde{B}(\mathbf{l}_1, \mathbf{l}_2, \mathbf{l}_3)\delta(\mathbf{l}_1 + \mathbf{l}_2 + \mathbf{l}_3) &= B(\mathbf{l}_1, \mathbf{l}_2, \mathbf{l}_3)\delta(\mathbf{l}_1 + \mathbf{l}_2 + \mathbf{l}_3) + \left(\langle T(\mathbf{l}_1)T(\mathbf{l}_2)[\nabla\psi \cdot \nabla T](\mathbf{l}_3) \rangle \right. \\ &\quad + \langle T(\mathbf{l}_1)[\nabla\psi \cdot \nabla T](\mathbf{l}_2)[\nabla\psi \cdot \nabla T](\mathbf{l}_3) \rangle \\ &\quad \left. + \frac{1}{2} \langle T(\mathbf{l}_1)T(\mathbf{l}_2)[\nabla^a\psi\nabla^b\psi\nabla_a T\nabla_b T](\mathbf{l}_3) \rangle + 2 \text{ perms} \right). \quad (32) \end{aligned}$$

One effect of the lensing terms is to generate a smoothing of features in the primordial bispectrum analogous to the effect in the power spectra [31,21]. This effect is not significant enough to affect the analysis of CMB data in the near future however [21].

A more important effect is due to the correlation of the CMB lensing potential with the large-scale temperature anisotropies. The CMB radiation we observe is redshifted or blueshifted by the evolution of potentials along the line of sight, a phenomenon often referred to as the (late-time) integrated Sachs-Wolfe (ISW) effect [32, 33]. The ISW contribution to the CMB anisotropies from linear potentials is significant at low multipoles ($\ell < 100$) due to the global effects of dark energy, but dies off rapidly on smaller scales. Since the evolving potentials that generate the ISW effect also cause lensing, there is some cross-correlation $C^{T\psi}$ between T and ψ , which is calculated in e.g. [25]. The correlation can be neglected for calculating the lensed power spectra, however a non-zero $C_l^{T\psi}$ generates a bispectrum, by the second term in Eq. (32), even if the primordial fluctuations are Gaussian [26,34]. At leading order in ψ this is given by

$$\langle \tilde{T}(\mathbf{l}_1)\tilde{T}(\mathbf{l}_2)\tilde{T}(\mathbf{l}_3) \rangle \approx -\frac{1}{2\pi}\delta(\mathbf{l}_1+\mathbf{l}_2+\mathbf{l}_3)(C_{l_1}^{T\psi}C_{l_2}^{TT}\mathbf{l}_1\cdot\mathbf{l}_2+5\text{ perms.}). \quad (33)$$

The value of this induced non-Gaussianity is greatest for “squeezed” triangles in which $l_1 \sim l_2 \gg l_3$ (or permutations thereof), corresponding to a large-scale temperature mode which is sourced by the ISW effect and two small-scale modes which are affected by lensing. This closely mimics the local form of non-Gaussianity which is predicted in a range of possible early-Universe scenarios (for a review, see [35]). For upcoming experiments such as Planck, this lensing-induced bispectrum will provide a large source of contamination for the measurement of primordial non-Gaussianity, and will need to be accurately accounted for to extract the primordial bispectrum [21, 36].

Note that because the lensing effects are linear in the observed CMB, lensing cannot generate a non-zero bispectrum in the absence of the $T\psi$ correlation, and the lowest order at which the lensing induces non-Gaussianity is the four-point correlation function or trispectrum. This has been studied thoroughly by several authors [37, 38].

5 Lens reconstruction

In the previous section we discussed how lensing affects the CMB power spectra and temperature bispectrum. We turn now to the issue of extracting more information about the lensing itself, in particular how to construct an optimal estimator for the lensing deflection field from the observed CMB. This reconstruction can then be connected to cosmological parameters with a likelihood analysis.

If we assume that the lensing potential is fixed then the statistics of the lensed CMB remain Gaussian, however the inhomogeneities which the lenses introduce make it statistically anisotropic. In Fourier space, this manifests itself as correlations between modes with $\mathbf{l} \neq \mathbf{l}'$, as we have already discussed. In real space, the manifestation is somewhat more intuitive: for an isotropic model, the correlation between two

points depends only on the distance between them, and the effect of the lens remapping is to make the observed, lensed distance between two points slightly larger or smaller than the primary, unlensed distance on which the correlation is defined. This feature may be exploited to produce estimators for the lensing potential. Consider, for example, the lensing expansion in Eq. (15), which shows that at first order in ψ the effect of lensing is to introduce a dependence into the observed CMB on the gradient of the unlensed CMB. This suggests that a quadratic estimator for the deflection angle of the form

$$\hat{\alpha}(\mathbf{x}) \propto \tilde{T}(\mathbf{x}) \nabla T(\mathbf{x}) \quad (34)$$

can be used to extract a measure of the lensing signal, if properly normalized. Taking the expectation value over realizations of the CMB, this estimator would recover the deflection field in the mean (at least to first order in the lensing expansion). The reconstruction is clearly quite noisy, however, as for any particular realization there will be some spurious $T\nabla T$ correlation in the unlensed CMB. Additionally, it is not clear how we would obtain the unlensed CMB $T(\mathbf{x})$ with which to perform the correlation. It is critical that the gradient of the unlensed CMB be used in Eq. (34) – if instead the gradient of the lensed CMB is used, the expectation value over CMB realizations vanishes to first order in ψ .

Here we will derive a more rigorous lensing estimator, by maximizing the likelihood of $\alpha(\mathbf{x})$ given the observed data, loosely following the approach of [39]. We will take the measurement to consist of noisy maps of T , Q and U measurements (or some subset thereof). We combine the observables at each point \mathbf{x} into a vector $\hat{\Theta}(\mathbf{x}) = \tilde{\Theta}(\mathbf{x}) + \mathbf{n}(\mathbf{x})$, where \mathbf{n} is the instrumental noise realization, which is also assumed to be Gaussian. The log-likelihood \mathcal{L} of the observed CMB is then given by

$$-\mathcal{L}(\hat{\Theta}|\alpha) = \frac{1}{2} \hat{\Theta}^T (\hat{C}^{\hat{\Theta}\hat{\Theta}})^{-1} \hat{\Theta} + \frac{1}{2} \ln \det(\hat{C}^{\hat{\Theta}\hat{\Theta}}), \quad (35)$$

where $\hat{C}^{\hat{\Theta}\hat{\Theta}}(\mathbf{x}, \mathbf{y}) = \tilde{C}^{\hat{\Theta}\hat{\Theta}}(\mathbf{x}, \mathbf{y}) + N(\mathbf{x}, \mathbf{y})$ is the covariance of the observation (including the effects of lensing) and we have left the integrals over positions implicit. We will construct an estimator for the deflection field by maximizing the likelihood with respect to the deflection field $\alpha(\mathbf{x})$. Taking the functional derivative of the likelihood with respect to the vector components α_i we find

$$\frac{\delta \mathcal{L}}{\delta \alpha_i(\mathbf{x})} = \frac{1}{2} \hat{\Theta}^T (\hat{C}^{\hat{\Theta}\hat{\Theta}})^{-1} \frac{\delta \hat{C}^{\hat{\Theta}\hat{\Theta}}}{\delta \alpha_i(\mathbf{x})} (\hat{C}^{\hat{\Theta}\hat{\Theta}})^{-1} \hat{\Theta} - \frac{1}{2} \text{Tr} \left[(\hat{C}^{\hat{\Theta}\hat{\Theta}})^{-1} \frac{\delta \hat{C}^{\hat{\Theta}\hat{\Theta}}}{\delta \alpha_i(\mathbf{x})} \right]. \quad (36)$$

The trace term results in a “mean field” over realizations of the unlensed CMB and noise. To see this, consider the identity $\text{Tr}(\mathbf{A}) = \langle \mathbf{x}^T \mathbf{A} \mathbf{C}^{-1} \mathbf{x} \rangle$, where \mathbf{A} is any matrix and \mathbf{x} is a vector of Gaussian random variables with covariance \mathbf{C} . Making this substitution with $\mathbf{C} = \hat{C}^{\hat{\Theta}\hat{\Theta}}$ and maximizing the likelihood by setting $\delta \mathcal{L} / \delta \alpha_i(\mathbf{x}) = 0$ gives the simple equation

$$\frac{\delta \mathcal{L}}{\delta \alpha_i(\mathbf{x})} = \mathcal{H}_i(\mathbf{x}) - \langle \mathcal{H}_i(\mathbf{x}) \rangle = 0, \quad (37)$$

where the components $\mathcal{H}_i(\mathbf{x})$ are given by

$$\mathcal{H}_i(\mathbf{x}) = \frac{1}{2} \left[(\tilde{C}^{\hat{\theta}\hat{\theta}})^{-1} \tilde{\Theta} \right]^T \frac{\delta \tilde{C}^{\hat{\theta}\hat{\theta}}}{\delta \alpha_i(\mathbf{x})} \left[(\tilde{C}^{\hat{\theta}\hat{\theta}})^{-1} \tilde{\Theta} \right]. \quad (38)$$

The values of $\delta \tilde{C}^{\hat{\theta}\hat{\theta}} / \delta \alpha_i(\mathbf{x})$ are calculated analytically from the $\mathcal{O}(\alpha)$ covariance in e.g. [40,41] (albeit with a slightly different notational convention than the one used here). Equation (37) may be solved iteratively using the Newton-Raphson method by updating $\alpha(\mathbf{x})$ according to

$$\delta \hat{\alpha}_i(\mathbf{x}) = - \int d\mathbf{y} \mathcal{A}_{ij}(\mathbf{x}, \mathbf{y}) [\mathcal{H}_j - \langle \mathcal{H}_j \rangle](\mathbf{y}), \quad (39)$$

where sub-scripted quantities are evaluated at the current estimate of $\alpha(\mathbf{x})$, and the normalization $\mathcal{A}_{ij}(\mathbf{x}, \mathbf{y})$ is given by

$$\mathcal{A}_{ij}(\mathbf{x}, \mathbf{y}) = \left[\frac{\delta^2 \mathcal{L}}{\delta \alpha_i(\mathbf{x}) \delta \alpha_j(\mathbf{y})} \right]^{-1} = \left[\frac{\delta}{\delta \alpha_i(\mathbf{x})} (\mathcal{H}_j - \langle \mathcal{H}_j \rangle)(\mathbf{y}) \right]^{-1}, \quad (40)$$

which in practice can be approximated by the Fisher matrix (see below). It is apparent that the quadratic term $\mathcal{H}(\mathbf{x})$ produces a measure of the deflection angle $\alpha(\mathbf{x})$. Note that in the absence of lensing, with homogeneous sky coverage we must have $\langle \mathcal{H}_i(\mathbf{x}) \rangle = 0$, as the expectation value would otherwise pick out a preferred direction on the sky [39].

In fact, $\mathcal{H}_i(\mathbf{x})$ is quite closely related to the heuristic estimator of Eq. (34). To show this, we begin by finding the derivative of the lensed CMB with respect to the deflection angle. This is straightforward since $\tilde{\Theta}(\mathbf{x}) = \Theta(\mathbf{x} + \alpha(\mathbf{x}))$, so

$$\frac{\delta}{\delta \alpha_i(\mathbf{y})} \tilde{\Theta}(\mathbf{x}) = \delta(\mathbf{x} - \mathbf{y}) (\nabla_i \Theta)(\mathbf{x} + \alpha(\mathbf{x})), \quad (41)$$

i.e. if the deflection angle is changed at a point, the lensed field only changes at the same point and by an amount that depends on the gradient of the unlensed fields $\nabla \Theta$ at the source position. To proceed further, it is useful to define the linear lensing operator $\Lambda(\mathbf{x}, \mathbf{y})$ such that the lensed CMB is given by $\tilde{\Theta}(\mathbf{x}) = \Theta(\mathbf{x} + \alpha(\mathbf{x})) = \int d^2\mathbf{y} \Lambda(\mathbf{x}, \mathbf{y}) \Theta(\mathbf{y})$, or explicitly

$$\Lambda(\mathbf{x}, \mathbf{y}) = \delta(\mathbf{x} + \alpha(\mathbf{x}) - \mathbf{y}). \quad (42)$$

With this notation the derivative of the lensed covariance $\tilde{C}^{\hat{\theta}\hat{\theta}} = \Lambda C^{\Theta\Theta} \Lambda^T$ (where $\Lambda^T(\mathbf{x}, \mathbf{y}) = \Lambda(\mathbf{y}, \mathbf{x})$) is given by

$$\frac{\delta}{\delta \alpha_i(\mathbf{x})} \tilde{C}^{\hat{\theta}\hat{\theta}}(\mathbf{y}, \mathbf{z}) = \delta(\mathbf{x} - \mathbf{y}) \int d^2\mathbf{y}' d^2\mathbf{z}' \Lambda(\mathbf{y}, \mathbf{y}') \nabla_{y'i} C^{\Theta\Theta}(\mathbf{y}', \mathbf{z}') \Lambda(\mathbf{z}, \mathbf{z}') + (\mathbf{y} \leftrightarrow \mathbf{z}). \quad (43)$$

Equation (38) then simplifies to a real-space operation on filtered fields [39]:

$$\mathcal{H}_i(\mathbf{x}) = \mathbf{F}_1^T(\mathbf{x}) (\nabla_i \mathbf{F}_2)(\mathbf{x} + \alpha(\mathbf{x})), \quad (44)$$

where the filtered fields are defined by

$$\mathbf{F}_1(\mathbf{x}) \equiv [(\hat{C}^{\hat{\theta}\hat{\theta}})^{-1}\hat{\Theta}](\mathbf{x}), \quad \mathbf{F}_2(\mathbf{x}) \equiv [C^{\Theta\Theta}\Lambda^T(\hat{C}^{\hat{\theta}\hat{\theta}})^{-1}\hat{\Theta}](\mathbf{x}). \quad (45)$$

The filtered field $\mathbf{F}_2 = \Lambda^{-1}\tilde{C}^{\tilde{\theta}\tilde{\theta}}(\hat{C}^{\hat{\theta}\hat{\theta}})^{-1}\hat{\Theta}$ is the Wiener reconstruction of the unlensed CMB, i.e. the optimal estimate of the unlensed CMB given the observed noisy data, the estimate of α and the unlensed CMB covariance matrix. The gradient term $(\nabla\mathbf{F}_2)(\mathbf{x} + \alpha(\mathbf{x}))$ is then just the best estimate of the unlensed gradient evaluated at the unlensed position, and this is contracted with the inverse-covariance-weighted lensed CMB at \mathbf{x} to form $\mathcal{H}_i(\mathbf{x})$. The weighting in \mathbf{F}_1 is typical of any optimal estimator of CMB observables and serves to down-weight the estimate in areas of high instrumental noise or cosmic variance. To understand why the $\nabla\mathbf{F}_2$ term is evaluated at the displaced position, let the true deflection field differ from the current estimate $\alpha(\mathbf{x})$ by $\delta\alpha(\mathbf{x})$. To linear order in $\delta\alpha(\mathbf{x})$, the lensed CMB at \mathbf{x} is

$$\tilde{\Theta}(\mathbf{x}) = \Theta(\mathbf{x} + \alpha(\mathbf{x})) + \delta\alpha^i(\mathbf{x})(\nabla_i\Theta)(\mathbf{x} + \alpha(\mathbf{x})). \quad (46)$$

It is therefore necessary to multiply by the gradient of the unlensed CMB at $\mathbf{x} + \alpha(\mathbf{x})$ to obtain an estimator which is proportional to the desired *change* in deflection field when averaged over realizations of the unlensed CMB.

We now consider the error on the reconstruction. The Fisher matrix,

$$\mathcal{F}_{ij}(\mathbf{x}, \mathbf{y}) = - \left\langle \frac{\delta^2 \mathcal{L}}{\delta\alpha_i(\mathbf{x})\delta\alpha_j(\mathbf{y})} \right\rangle = \frac{1}{2} \text{Tr} \left[(\hat{C}^{\hat{\theta}\hat{\theta}})^{-1} \frac{\delta\tilde{C}^{\tilde{\theta}\tilde{\theta}}}{\delta\alpha_i(\mathbf{x})} (\hat{C}^{\hat{\theta}\hat{\theta}})^{-1} \frac{\delta\tilde{C}^{\tilde{\theta}\tilde{\theta}}}{\delta\alpha_j(\mathbf{y})} \right], \quad (47)$$

provides a lower bound on the variance of an unbiased estimate of α by the Cramer-Rao inequality. The expectation value in Eq. (47) is taken over realizations of the CMB and noise for fixed lenses. This may be evaluated analytically at $\alpha = 0$ if we have isotropic sky coverage, in which case we find

$$\begin{aligned} \mathcal{F}_{ij}^{(0)}(\mathbf{x}, \mathbf{y}) = & \int d^2\mathbf{x}' d^2\mathbf{y}' \text{Tr} \left[(\hat{C}^{\hat{\theta}\hat{\theta}})^{-1}(\mathbf{x}', \mathbf{x}) \nabla_{x'i} C^{\Theta\Theta}(\mathbf{x}, \mathbf{y}') (\hat{C}^{\hat{\theta}\hat{\theta}})^{-1}(\mathbf{y}', \mathbf{y}) \nabla_{y'j} C^{\Theta\Theta}(\mathbf{y}, \mathbf{x}') \right. \\ & \left. + (\hat{C}^{\hat{\theta}\hat{\theta}})^{-1}(\mathbf{y}, \mathbf{x}) \nabla_{x'i} C^{\Theta\Theta}(\mathbf{x}, \mathbf{y}') (\hat{C}^{\hat{\theta}\hat{\theta}})^{-1}(\mathbf{y}', \mathbf{x}') \nabla_{y'j} C^{\Theta\Theta}(\mathbf{x}', \mathbf{y}) \right]_{\alpha=0}. \quad (48) \end{aligned}$$

This is diagonal in Fourier space in its spatial arguments; for example, for the temperature alone we have

$$\begin{aligned} \mathcal{F}_{ij}^{(0)}(\mathbf{x}, \mathbf{y}) = & \int \frac{d^2\mathbf{L}}{(2\pi)^2} e^{i\mathbf{L}\cdot(\mathbf{x}-\mathbf{y})} N_{ij}^{-1}(\mathbf{L}) \\ \text{where } N_{ij}^{-1}(\mathbf{L}) \equiv & \frac{1}{2} \int \frac{d^2\mathbf{l}}{(2\pi)^2} \frac{[(\mathbf{L}-\mathbf{l})C_{|\mathbf{l}-\mathbf{L}|}^{TT} + \mathbf{l}C_l^{TT}]_i [(\mathbf{L}-\mathbf{l})C_{|\mathbf{l}-\mathbf{L}|}^{TT} + \mathbf{l}C_l^{TT}]_j}{(C_l^{TT} + N_l)} \frac{1}{(C_{|\mathbf{l}-\mathbf{L}|}^{TT} + N_{|\mathbf{l}-\mathbf{L}|})}. \quad (49) \end{aligned}$$

Here, N_l is the noise power spectrum of the temperature map. To make contact with previous work [14,40] that reconstructed the lensing potential ψ rather than

the deflection field, we note that the Fisher matrix $\mathcal{F}_\psi^{(0)}$ is related to that for α by $\mathcal{F}_\psi^{(0)}(\mathbf{x}, \mathbf{y}) = \nabla_{y,i} \nabla_{x,j} \mathcal{F}_{ij}^{(0)}(\mathbf{x}, \mathbf{y})$. Equation (49) then gives

$$\mathcal{F}_\psi^{(0)}(\mathbf{x}, \mathbf{y}) = \int \frac{d^2 \mathbf{L}}{(2\pi)^2} e^{i\mathbf{L} \cdot (\mathbf{x} - \mathbf{y})} \left[\frac{1}{2} \int \frac{d^2 \mathbf{l}}{(2\pi)^2} \frac{[\mathbf{L} \cdot (\mathbf{l} - \mathbf{l}) C_{|\mathbf{l} - \mathbf{l}|}^{TT} + \mathbf{L} \cdot \mathbf{l} C_l^{TT}]^2}{(C_l^{TT} + N_l)(C_{|\mathbf{l} - \mathbf{l}|}^{TT} + N_{|\mathbf{l} - \mathbf{l}|})} \right], \quad (50)$$

which agrees with the power spectrum of the reconstruction noise derived for the optimal quadratic estimator of ψ in [40] in the limit of no lensing. Note that in reconstructing α rather than ψ we allow for the possibility of a curl mode in α . This can act as a monitor for systematic effects, as it is expected to be zero cosmologically. However constraints using the iterated estimator can be improved by using a prior that it is zero [14].

We will refer to the Fisher noise level at $\alpha = \mathbf{0}$ as the ‘‘Fisher limit’’; it is plotted for two instrumental noise levels in Fig. 5. In practice, the reconstruction noise can be larger than the Fisher limit due to the confusion created by the lenses themselves, which act as a source of noise in the observed CMB and make the lensing likelihood slightly non-Gaussian [14]. For temperature and E -mode polarization reconstruction these effects are generally negligible, as the lensing represents a small perturbation to the primary signal. For a reconstruction including B -mode polarization measurements, however, the difference is very important at low noise levels as the lensing contributions constitute a significant fraction of the observed B -mode power. The true reconstruction noise can be determined from simulations [14]. In [42] it is shown that a good approximation to the true error may be obtained by treating the contribution of poorly constrained modes of ψ to be Gaussian. This is done by replacing the unlensed power spectra in the denominator of Eq. (50) with the spectra of the partially de-lensed CMB. The amount of de-lensing which is possible is in turn determined by the lens reconstruction noise (and so the reconstruction noise calculation must be iterated until convergence). We follow this approach to calculate the noise curves in Fig. 5.

On small scales CMB lensing can also be used to study individual clusters; here the unlensed CMB is nearly a pure gradient, and the cluster signal is a small ‘‘wiggle’’ in this gradient due to the deflection by the cluster. However the signal-to-noise on single clusters is generally low, and for temperature lensing there are several sources of confusion (see, for example, Refs. [43,44]).

6 Experimental status and prospects

The experimental evidence for CMB lensing has developed greatly in the past several years. At the power spectrum level, lensing causes $\mathcal{O}(10\%)$ effects at $l > 1000$ which are now becoming testable with small-scale experiments. The ACBAR team have fit for the amplitude of lensing effects in their parameter analysis of ACBAR and WMAP data and find a peak within one-sigma of the expected value (although the lensing amplitude is still consistent with zero at the percent level) [45]. An optimal analysis of lensing effects should produce a more significant detection, but requires stringent control of instrumental systematic effects and foregrounds. Thus far, such

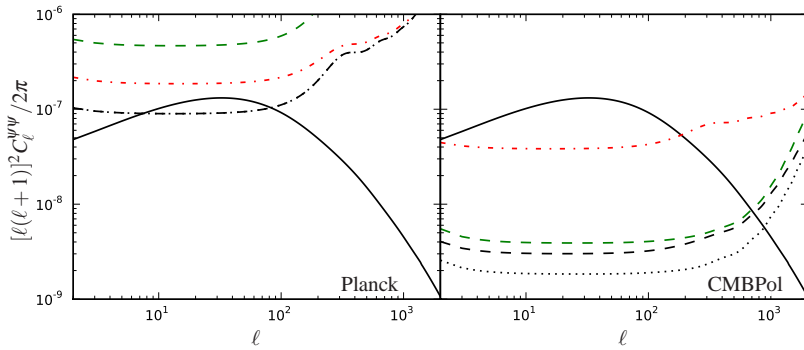


Fig. 5 Power spectrum of the errors in the gradient part of the reconstructed deflection field for two full-sky experiments. Left: an approximation to the Planck satellite, with $\sigma(T) = 27 \mu\text{K}\cdot\text{arcmin}$. Right: a version of the proposed CMBPol mission, with $\sigma(T) = 1 \mu\text{K}\cdot\text{arcmin}$. For both experiments, we assume a Gaussian beam of FWHM 7 arcmin and Q and U noise levels equal to $\sqrt{2}\sigma(T)$. The curves are the theory deflection power (solid black), reconstruction errors from temperature alone (red dot-dashed), polarization alone (green dashed), temperature and polarization together (black dashed), and the Fisher limit (black dotted). For Planck, the Fisher limit is saturated.

an analysis has only been performed for the temperature data of the WMAP satellite. The WMAP data only extends to $l_{\text{max}} \sim 500$, and so does not contain enough small-scale data to reconstruct the lensing potential with good signal-to-noise. By cross-correlating a lens reconstruction from the WMAP data with a lower-noise tracer of the large-scale structure (LSS), however, it is possible to obtain an overall detection. This was first attempted by [46], who found no detection of lensing effects in cross-correlation with the luminous red galaxies (LRGs) of the Sloan Digital Sky Survey (SDSS). Their result was improved upon by [47], who used radio sources from the NRAO VLA Sky Survey (NVSS), which has a better redshift overlap with the structures which lens the CMB. They found a 3.4σ detection of lensing. Finally, [48] have improved their original analysis by incorporating correlation with NVSS sources as well as quasars from the SDSS survey. They use a more conservative cut of the NVSS sources and a slightly sub-optimal estimator compared to [47], obtaining evidence for the expected lensing-LSS correlation of 2.5σ . All three of these cross-correlation results have incorporated very thorough tests for both instrumental and astrophysical systematics, most of which have negligible effects on the current overall error budget.

At present, therefore, there is experimental evidence at modest significance for the effect of gravitational lensing in the CMB. High-resolution experiments which are currently taking data, such as Planck, ACT, and SPT, are expected to improve this situation dramatically, with reconstruction signal-to-noise approaching unity for many modes of the ψ field. This will enable CMB lensing to become a useful tool for precision cosmology. With lens reconstruction from the Planck data, for example, constraints on the energy density of massive neutrinos are expected to improve by a factor of two over an analysis which neglects a lensing reconstruction [5, 6, 49]. CMB lensing measurements will also enable definitive testing between some theoretical models of the anomalous CMB “cold spot” [50]. Upcoming large-scale polarization

experiments, such as BICEP2, QUIET, and PolarBeaR, are also expected to detect lensing in polarization through the B -modes which it induces.

As CMB lensing moves from a purely theoretical study to an observational one, there are a number of challenges to be overcome. The effects of foregrounds, such as the Sunyaev-Zel'dovich effect and residual extra-Galactic point-sources, will become increasingly important as high signal-to-noise detections of lensing are attempted. The construction of a realistic lensing likelihood for the purpose of parameter constraints has also yet to be demonstrated. In the more distant future, CMB lensing should provide the dominant source of confusion for primordial B -mode measurements targeting the signal from recombination around $l \sim 100$ (for sufficiently low tensor amplitude). Lens reconstruction with polarization and delensing will become important tools to mitigate this confusion, and preliminary work on these techniques and their sensitivity to foregrounds and instrumental systematics is currently under active development [42].

Acknowledgements DH is supported by a Gates' Scholarship. AL acknowledges an STFC Advanced Fellowship.

References

1. D.J. Fixsen, J.C. Mather, *Astrophys. J.* **581**, 817 (2002).
2. W. Hu, M.J. White, *New Astron.* **2**, 323 (1997). astro-ph/9706147.
3. L. Knox, Y.S. Song, *Phys. Rev. Lett.* **89**, 011303 (2002). astro-ph/0202286.
4. U. Seljak, C.M. Hirata, *Phys. Rev.* **D69**, 043005 (2004). astro-ph/0310163.
5. M. Kaplinghat, L. Knox, Y.S. Song, *Phys. Rev. Lett.* **91**, 241301 (2003). astro-ph/0303344.
6. J. Lesgourgues, L. Perotto, S. Pastor, M. Piat, *Phys. Rev.* **D73**, 045021 (2006). astro-ph/0511735.
7. R. de Putter, O. Zahn, E.V. Linder, *Phys. Rev.* **D79**, 065033 (2009). 0901.0916.
8. B. Partridge, *3K: The Cosmic Microwave Background Radiation*. Cambridge Astrophysics Series (Cambridge University Press, 1995)
9. U. Seljak, M. Zaldarriaga, *Phys. Rev. Lett.* **78**, 2054 (1997). astro-ph/9609169.
10. M. Kamionkowski, A. Kosowsky, A. Stebbins, *Phys. Rev. Lett.* **78**, 2058 (1997). astro-ph/9609132.
11. A. Lewis, A. Challinor, *Phys. Rept.* **429**, 1 (2006). astro-ph/0601594.
12. A. Cooray, W. Hu, *Astrophys. J.* **574**, 19 (2002). astro-ph/0202411.
13. C. Shapiro, A. Cooray, *JCAP* **0603**, 007 (2006). astro-ph/0601226
14. C.M. Hirata, U. Seljak, *Phys. Rev.* **D68**, 083002 (2003). astro-ph/0306354.
15. S. Das, P. Bode, *Astrophys. J.* **682**, 1 (2008). 0711.3793
16. R.E. Smith, et al., *Mon. Not. Roy. Astron. Soc.* **341**, 1311 (2003). astro-ph/0207664.
17. A. Lewis, A. Challinor, A. Lasenby, *Astrophys. J.* **538**, 473 (2000). astro-ph/9911177.
18. C. Carbone, C. Baccigalupi, M. Bartelmann, S. Matarrese, V. Springel, *Mon. Not. Roy. Astron. Soc.* **396**, 668 (2009). 0810.4145.
19. P. Fosalba, E. Gaztanaga, F. Castander, M. Manera, *Mon. Not. Roy. Astron. Soc.* **391**, 435 (2008). 0711.1540
20. A. Challinor, G. Chon, *Phys. Rev.* **D66**, 127301 (2002). astro-ph/0301064.
21. D. Hanson, K.M. Smith, A. Challinor, M. Liguori, *Phys. Rev.* **D80**, 083004 (2009). 0905.4732.
22. U. Seljak, *Astrophys. J.* **463**, 1 (1996). astro-ph/9505109.
23. M. Zaldarriaga, U. Seljak, *Phys. Rev.* **D58**, 023003 (1998). astro-ph/9803150.
24. A. Challinor, A. Lewis, *Phys. Rev.* **D71**, 103010 (2005). astro-ph/0502425.
25. W. Hu, *Phys. Rev.* **D62**, 043007 (2000). astro-ph/0001303.
26. M. Zaldarriaga, *Phys. Rev.* **D62**, 063510 (2000). astro-ph/9910498.
27. K.M. Smith, W. Hu, M. Kaplinghat, *Phys. Rev.* **D74**, 123002 (2006). astro-ph/0607315.
28. S. Smith, A. Challinor, G. Rocha, *Phys. Rev.* **D73**, 023517 (2006). astro-ph/0511703.
29. C. Li, T.L. Smith, A. Cooray, *Phys. Rev.* **D75**, 083501 (2007). astro-ph/0607494.

-
30. N. Bartolo, E. Komatsu, S. Matarrese, A. Riotto, Phys. Rept. **402**, 103 (2004). astro-ph/0406398.
 31. A. Cooray, D. Sarkar, P. Serra, Phys. Rev. **D77**, 123006 (2008). 0803.4194.
 32. R.K. Sachs, A.M. Wolfe, Ap. J **147**, 73 (1967).
 33. M.J. Rees, D.W. Sciama, Nature **217**, 511 (1968).
 34. D.M. Goldberg, D.N. Spergel, Phys. Rev. **D59**, 103002 (1999). astro-ph/9811251.
 35. J.R. Fergusson, E.P.S. Shellard, Phys. Rev. **D80**, 043510 (2009). 0812.3413.
 36. P. Serra, A. Cooray, Phys. Rev. **D77**, 107305 (2008). 0801.3276.
 37. W. Hu, Phys. Rev. **D64**, 083005 (2001). astro-ph/0105117.
 38. M.H. Kesden, A. Cooray, M. Kamionkowski, Phys. Rev. **D67**, 123507 (2003). astro-ph/0302536.
 39. C.M. Hirata, U. Seljak, Phys. Rev. **D67**, 043001 (2003). astro-ph/0209489.
 40. W. Hu, T. Okamoto, Astrophys. J. **574**, 566 (2002). astro-ph/0111606.
 41. T. Okamoto, W. Hu, Phys. Rev. **D67**, 083002 (2003). astro-ph/0301031.
 42. K.M. Smith, et al., AIP Conference Proceedings **1141**, 121 (2008). 0811.3916
 43. U. Seljak, M. Zaldarriaga, Astrophys. J. **538**, 57 (2000). astro-ph/9907254.
 44. J. Yoo, M. Zaldarriaga, Phys. Rev. **D78**, 083002 (2008). 0805.2155.
 45. C.L. Reichardt, et al., Astrophys. J. **694**, 1200 (2009). 0801.1491.
 46. C.M. Hirata, N. Padmanabhan, U. Seljak, D. Schlegel, J. Brinkmann, Phys. Rev. **D70**, 103501 (2004). astro-ph/0406004.
 47. K.M. Smith, O. Zahn, O. Dore, Phys. Rev. **D76**, 043510 (2007). 0705.3980.
 48. C.M. Hirata, S. Ho, N. Padmanabhan, U. Seljak, N.A. Bahcall, Phys. Rev. **D78**, 043520 (2008). 0801.0644.
 49. L. Perotto, J. Lesgourgues, S. Hannestad, H. Tu, Y.Y.Y. Wong, JCAP **0610**, 013 (2006). astro-ph/0606227
 50. S. Das, D.N. Spergel, Phys. Rev. **D79**, 043007 (2009). 0809.4704.